Experimental Studies of Amorphous and Polycrystalline Ice Films Using FT-RAIRS

Belén Maté,* Alicia Medialdea, Miguel A. Moreno, Rafael Escribano, and Victor J. Herrero*

Instituto de Estructura de la Materia (CSIC), Serrano 121-123, 28006 Madrid, Spain

Received: February 20, 2003; In Final Form: July 2, 2003

A systematic investigation of amorphous and crystalline vapor deposited ice layers with thickness ranging from less than 100 nm to more than 5 μm has been performed using Fourier transform (FT) reflection−absorption infrared spectroscopy (RAIRS). Al and Au surfaces were used for the vapor deposition and very similar results were obtained on both. The spectra were recorded both with polarized and nonpolarized radiation and simulated with a simple Fresnel reflection model and empirical optical indices from the literature. Optical effects peculiar to this technique like surface suppression or enhancement of vibrational modes, saturation of intense absorptions, and IR interferences, are found to distort the spectra to a greater or lesser extent over the whole thickness range investigated. The diverse spectral band shapes and intensities are globally well reproduced with the mentioned Fresnel model. Some noteworthy discrepancies are, however, observed in the most intense peaks of the polarized spectra, which are affected by larger distortions. Whenever possible, the present measurements have been compared with published spectra recorded under similar conditions and a good accordance has been found. This comparison and the spectral simulations can reconcile seeming discrepancies in the previous literature data.

1. Introduction

Ice particles are known to play a key role in a great variety of physical and chemical processes taking place in different regions of the atmosphere as well as in comets and in the interstellar space.[1−5]

The very peculiar ability of water to form different networks of hydrogen bonds gives rise to various types of condensed phases (see for instance refs 6−8 and references therein), which depend on the formation conditions. Extensive experimental studies by many research groups have shown that the deposition of low-pressure water vapor below 150 K can lead to the generation of two amorphous solids and a viscous liquid. At $T \approx 150$ K a cubic polycrystalline ice, I_c, can form and above 160 K a hexagonal polycrystalline form, I_h, can also appear. Crystalline and noncrystalline phases can apparently coexist till temperatures as high as 210 K.[9] The experimental techniques used for the study of the structure of these ice phases and the transformations between them include X-ray,[10−12] electron[7,9,13] and neutron diffraction,[14,15] inelastic scattering of neutrons,[16] electrons,[17] and He atoms,[18] calorimetry,[19] thermal desorption,[8,9,17,20−28] and IR and Raman vibrational spectroscopy.[29−44] Despite the wide variety of techniques applied and of the continuing efforts devoted to the problem, there are still many open questions regarding the structure and properties of low-pressure ice (ice I).

IR absorptions in ice have been reported in the scientific literature at least since the beginning of the 20th century[45] and Raman spectra have been available since the 1920s.[46] Assignments of the vibrational spectrum of ice I (both amorphous and crystalline), summarizing most previous work, were provided in the 1960s and 1970s.[29,30,47] The distinct spectral features over the 200−3600 cm^{-1} range were described in terms of vibrational modes of individual water molecules, of lattice vibrations, or of combinations of them. In later works a small absorption peak at 3690−3700 cm^{-1} present in the spectra of both ice films and clusters[30,36,40,44,48−52] was attributed to the stretching of incompletely coordinated OH groups ("dangling bonds") either at the outer solid surface or at the internal surfaces of micropores.

Particular attention has been paid to the region around ≈2800−3600 cm^{-1} associated with OH stretching vibrations of bulk ice. To justify the changes in the band shapes measured with different Raman polarizations and with IR transmission spectroscopy, Whalley[47] assumed an ordered model of ice and explained the various features observed as collective symmetric (ν_1) and antisymmetric (ν_3) OH stretching vibrations oscillating in or out of phase, and being subject to a splitting in energy between longitudinal (LO) and transverse (TO) optic modes. The splitting was caused by the long-range electric field arising from the transition moments of the molecules. The magnitude of the LO/TO splitting was estimated, as a function of the limiting high- and low-frequency refractive indices of the infrared band, by the generalized Lyddane−Sachs−Teller (LST) relation.[53]

More refined theoretical treatments of this spectral region by Rice and co-workers[54−56] questioned the description in terms of single molecule vibrations, stressed the importance of the coupling between inter- and intramolecular vibrations and pointed at the significant role of disorder in the observed spectra. They noted also a possible (small) influence of a Fermi resonance between the OH stretching motion and the first bending overtone on the observed Raman bands. These authors recognized the influence of long-range macroscopic fields in altering the states of the system but considered that a simple TO/LO mode separation model could not account for the complex system behavior and found no evidence for linking structure in vibrational spectra with specific modes caused by macroscopic fields.

Recently, Buch and Devlin[43] have proposed a new interpretation of the OH-stretch spectrum of ice. In analogy with Whalley, these authors started with an ordered model, but instead of taking

* Corresponding authors. E-mail: bmate@iem.cfmac.csic.es, vherrero@iem.cfmac.csic.es.

10.1021/jp0344343 CCC: $25.00
Published on Web 09/16/2003

collective vibrations of single molecules they considered that the relevant basic unit was composed of four oscillating dipoles in a tetrahedral arrangement around an O atom. Disorder was then introduced as a perturbation and sample geometries were contemplated in the calculations. For slab geometries, the model predicted a splitting of the OH modes into a transverse (T) and a longitudinal/intermediate (L/I) band caused by coupling of the macroscopic field with individual dipoles. The various groups of modes associated with the OH stretch vibrations can be made manifest with suitable experimental arrangements, and in fact, the model could account for the differences observed in the band shapes of IR spectra of particles, and of polarized Raman and IR transmission spectra of thin films.[43]

In general, progress toward a precise theoretical description of the vibrational spectra of ice is hampered not only by the intrinsic difficulty of the problem, but also by the disparity of experimental results arising from the polymorphism of the micro-phases present in most samples and from peculiarities of the different techniques employed.

Reflection−absorption infrared spectroscopy (RAIRS), a well-established technique for the study of adsorbates on metal surfaces, has been used by several groups[9,37,40,42,44] for the investigation of vapor deposited ice layers. In this method a beam of IR radiation is subjected to a reflection from the film−substrate system.[57] The reflection−absorption (RA) signals depend not only on the absorbing properties of the sample but also on the reflection geometry and on the polarization of the radiation.[58,59] This dependence can be used advantageously for many investigations, providing an adequate model is employed to account for the optical effects inherent to the method. On the other hand, a careful consideration of scattering and reflection effects can be very useful for the interpretation of field measurements in the atmosphere.

Horn et al.[37] addressed the influence of optical effects on the grazing angle (75°) RAIR spectra of amorphous H_2O and D_2O ice layers of different thickness (estimated to vary between 50 nm and several micrometers) deposited on a gold substrate at 90 K. With increasing thickness the absorption band in the OH stretching region was found first to broaden and then to develop a notch at the top. The optical properties of the multiphase (metal/ice/vacuum) system were modeled within a classical formalism based on Fresnel equations[59,60] using the refractive indices of Toon et al.[61] The authors invoked the LTS splitting[53,62] between LO and TO modes to rationalize the changes observed in the OH stretching region with increasing film thickness. By summing the model band shapes calculated for IR radiation polarized parallel (s) or perpendicular (p) to the deposition surface, Horn et al. obtained band contours similar to the (unpolarized) experimental ones, but with much higher intensities. The discrepancy between calculated and observed intensity was attributed to the lack of sophistication used in the model,[59] which had been developed for homogeneous films. In a later work, Jenniskens et al.,[9] using the same experimental setup, investigated the behavior of ultrathin (<50 nm) amorphous films upon prolonged (55 min) annealing at 160 K and found changes in the band shape similar to those observed previously in amorphous films with increasing thickness.[37]

Zondlo et al.[40] measured s- and p-polarized grazing-angle (83°) RAIR spectra of polycrystalline ice films deposited on an Al surface at 163 K. They used also a Fresnel model[58] to simulate the absorption contours in the OH stretching region. The simulated band shapes were in good agreement with the measured ones, over the thickness range studied (0.1−1 μm), but in most spectra, the calculated absorbances were smaller than the experimental ones. Zondlo et al.[40] noted that for similar shapes of the calculated polarized bands, their thickness values, which had been independently determined both from exposure and from optical interference measurements, were much smaller than those calculated in the work of Horn et al.[37] In a later work, Robinson et al.[63] used IR interference fringes between 6000 and 4095 cm^{-1} measured with grazing angle polarized RAIRS, to determine the thickness of ice layers in the 0.5−1.4 μm rage. The treatment used for the simulation of the spectra was analogous to that of Zondlo et al.[40] and also in this case a good agreement was obtained in the band shapes but the experimental absorbances were found to be appreciably larger than the calculated ones. The authors attributed also the discrepancy to the simplicity of the simulation model[58] originally developed for isotropic films.

In a recent work, Mitlin and Leung[44] used also grazing angle (83°) nonpolarized RAIRS to investigate the evolution of the OH stretch band and dangling bond feature with film thickness and temperature. Their films were deposited on a Cu substrate at temperatures between 128 and 185 K. A Mie scattering formalism was found to be preferable than the mentioned Fresnel reflection model to reproduce some of the spectra obtained in the very early deposition stages. This fact was taken as an indication of the heterogeneous character of the early deposit formed probably by nanoscale sized aggregates. In contrast to the results mentioned in the previous paragraphs[37,40,63] the Fresnel model was found to reproduce well not only the experimental band shapes but also the intensities of films with a thickness of 50 nm or larger (up to 1.4 μm, which were the thickest studied). Optical interference measurements were reported to yield thickness values in reasonable agreement with those used for the simulations of the nonpolarized spectra, and the authors concluded that the thickness parameter of the Fresnel model could be used as a semiempirical estimate of the actual film thickness. Mitlin and Leung showed also how the intensities and shapes of specific bands in the RA spectrum could be significantly affected by interference peaks that migrate with increasing thickness, complicating spectral identification. On the other hand, the spectral band contours of very thin films (<50 nm) directly deposited at 160 K were found to be at variance with those reported by Jenniksens at al.[9] for films of comparable thickness deposited initially at 90 K and then annealed for a long time at 160 K.

The observations of the previous paragraphs cast doubts and stress complications inherent to the interpretation of the RAIR spectra of ice. In an attempt to clarify some of the existing doubts and to delimit the contribution of the various optical effects to the RAIR spectra of ice films, we have performed systematic measurements of polarized and nonpolarized RAIR spectra of amorphous and polycrystalline vapor-deposited ice over Al and Au substrates. The thicknesses of the various ice films have been determined using optical interference measurements and have also been estimated from calculated deposition rates and deposition times. Special emphasis has been placed on the measurement and modeling of the spectra of thick layers (up to ≈5 μm) for which literature data are more scarce and controversial. The results are discussed and compared to previous works.

2. Experimental Section

The experimental system used in the present work is described elsewhere[64] and only the relevant details will be given here. A scheme of the system is presented in Figure 1. The experiment was conducted in a UHV cylindrical chamber evacuated by a

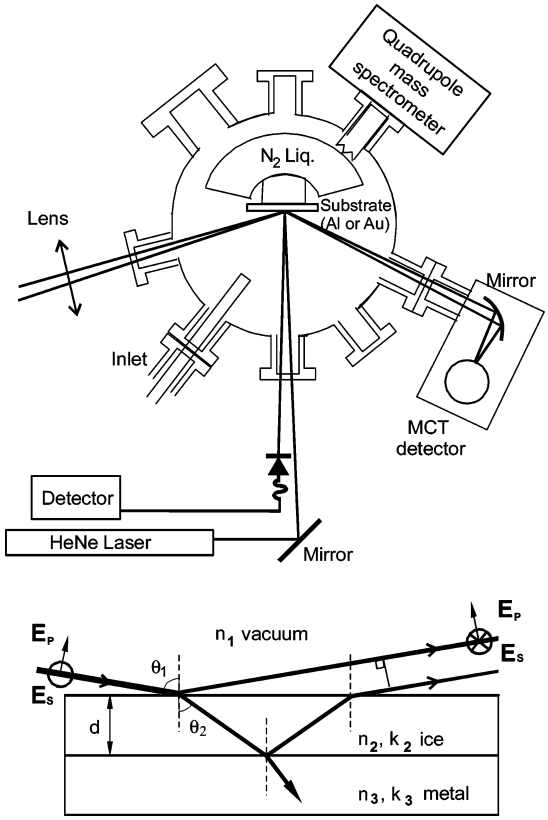

Figure 1. Upper part: scheme of the experimental set-up. Lower part: scheme of the interaction of the three layered vacuum/ice/metal system with the IR radiation E_p, E_s indicate p- and s-polarized components of the electric IR field (see text).

turbomolecular pump to a base pressure lower than 3×10^{-8} mbar and provided with a liquid nitrogen Dewar in contact with the deposition substrate. After filling the liquid nitrogen Dewar the base pressure was in the 10^{-9} range. To obtain a uniform deposition during the production of the ice samples, the gas inlet was not directed to the substrate surface but deviated to the wall by means of a curved ending so that the whole chamber was filled homogeneously with a small pressure of water vapor. The cold deposition surfaces were made of polished aluminum or gold. The surface temperature could be regulated between 80 and 323 K with an accuracy of 1 K. For the deposition of amorphous or crystalline ice films the substrate was kept either at 87 K or at 163 K, and the chamber was filled with a pressure of water vapor in the 6×10^{-6} to 3×10^{-5} mbar range during a controlled time. The water pressures were measured with a calibrated INFICON Transpector-2 quadrupole mass spectrometer, QMS (see next section for the calibration procedure). Deposition times varied from about 30 s for the thinnest films to 55 min for the thickest ones. It is generally assumed that the deposition of water vapor at 87 K will lead to the formation of low-density amorphous ice. At 163 K it should contain cubic crystalline ice, but crystalline and noncrystalline microphases could coexist in principle.[9] We will adhere to the common denomination and will refer to this deposit as crystalline or polycrystalline ice.

A FTIR spectrometer Bruker IFS66 was used to record the spectra. The IR radiation was focused on the sample with a CaF_2 (or a KBr) lens and the incidence angle was 75°. For a series of spectra a CaF_2 lens was used and the lower limit of the spectral range was approximately 1000 cm^{-1}. For other series of spectra we used a KBr lens, which sets a lower limit of approximately 400 cm^{-1}. The reflected IR light was focused by a curved mirror onto a mercury cadmium telluride (MCT) detector cooled with liquid nitrogen. A polarizer SPECAC KRS-5 placed before the focusing lens was used to select the incident radiation with an electric field vector parallel (p) or perpendicular (s) to the incidence plane to record the corresponding s- or p-polarized spectra. Each spectrum was obtained from the addition of two series of 512 scans, recorded at 8 cm^{-1} apodized resolution.

3. Film Thickness Determination

An optical interference system based on a He−Ne laser (632.8 nm) has been employed to determine the thickness of the ice films. This technique has been used previously by a number of groups.[21,24,40,44,65] The interference measurements were performed by monitoring the reflectance of the He−Ne laser incident on a growing ice film at $\theta_i = 4.0 \pm 0.2°$ from the surface normal (see Figure 1). The reflected light was detected by a photodiode and converted to a digital signal. Constructive and destructive interferences could be observed between the reflections from the vacuum−ice and the ice−metal interfaces. Constructive interference occurs when the path length difference between the two beams is an integral number, m, of wavelengths. The thickness of the film at constructive interference fringes is given by[21,24,40,65]

$$x = m\lambda \cos \theta_2 / 2(n_2(T) - n_1 \sin \theta_1 \sin \theta_2) \qquad (1)$$

where $\lambda = 632.8$ nm is the wavelength of the incident light, θ_2 is the angle of the transmitted beam with respect to the surface normal, n_1 is the refractive index of vacuum, and $n_2(T)$ is the temperature-dependent refractive index of the ice film. By using $n_1 = 1$ and $n_2(90K) = 1.27$ or $n_2(160K) = 1.31$ (ref 24), the solution of eq 1 leads to 249.5 or 242.2 nm, respectively, for the first constructive interference. In the present work thickness values up to ≈ 5 μm have been measured using this technique. Due to the experimental uncetainty in the amplitude of the interferences, film thickness values smaller than the first interference minimum, $d < 120$ nm, cannot be properly determined with this technique.

An independent estimate of the film thickness could be obtained from exposure. Using simple arguments from gas kinetic theory and assuming zero-order kinetics for the evaporation of ice, the approximate growth rate can be expressed as[21,24,40]

$$\frac{dx}{dt} = \frac{\alpha P_g}{\rho(T_s)\sqrt{2\pi m_g k T_g}} - \frac{\upsilon_0}{\rho(T_s)} \exp\left(-\frac{E_d}{RT_s}\right) \qquad (2)$$

where α is the condensation coefficient, P_g and T_g are the pressure and temperature of the gas (water vapor) in the chamber, T_s is the substrate temperature, $\rho(T_s)$ is the ice density corresponding to this temperature, m_g is the mass of the gas molecules, k is the Boltzmann constant, ν_0 is the zero-order desorption preexponential, and E_d is the desorption activation energy.

Condensation and evaporation on ice surfaces have been studied by several groups (see refs 8, 9, 20, 21,24, 28, and 66 and references therein). For the substrate temperatures ($T_s =$ 87 and 163 K) and gas pressures ($P_g > 5 \times 10^{-6}$ mbar) used in the present experiments, the condensation coefficient is expected to be[24] $\alpha \approx 1$. For the deposition of films at 87 K the evaporation is extremely slow and the second term of eq 2 can be neglected virtually always. However, at 163 K, evaporation may become important for low deposition rates.

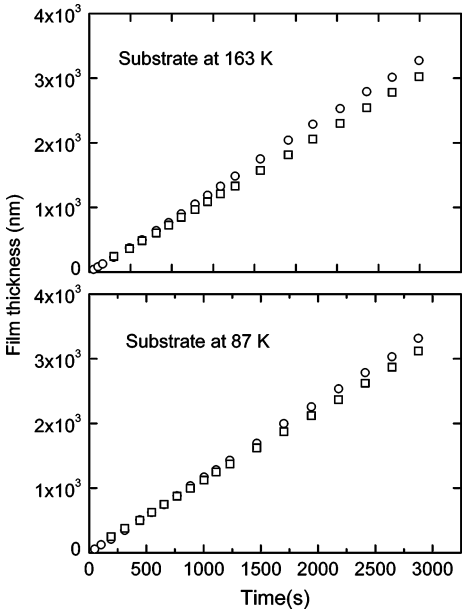

Figure 2. Film growth of amorphous (lower panel) and polycrystalline (upper panel) ice films. The water vapor pressure in the chamber was 8 x 10^{-6} mbar. Open squares: optical interference measurements obtained from eq. 1. Open circles: estimates from calculated deposition and evaporation rates from eq 2 with the parameters given in the text.

The measurement of the absolute pressure, P_g, of water in the 6×10^{-6} to 3×10^{-5} mbar range employed for the deposition, required a calibration of the quadrupole mass spectrometer used for the analysis of partial pressures. The calibration was performed in two stages. First the pumping speed of the turbomolecular pump for water vapor was determined by allowing a known flow of the vapor through a calibrated needle valve until the pressure in the chamber reached values in the $10^{-4}-10^{-3}$ mbar range (as measured with a capacitance manometer). From these measurements the pumping speed was determined in the stable ("flat") regime of the pump. The value of the pumping speed thus obtained can be safely extrapolated to lower chamber pressures. When the flow of H_2O vapor into the chamber was further reduced, the range of relevant pressures was attained. The pressure readings of the QMS (without electron multiplier) for a mass/charge ratio (m/q) of 18 were then compared to those calculated from the vapor flow and pumping speed and a calibration curve was obtained. The calculated pressures were nearly identical to the QMS readings for $P_g = 5 \times 10^{-6}$ mbar and then deviated gradually with increasing pressure. For a (corrected) P_g of 3×10^{-5} mbar, which was the highest pressure used in the experiments, the QMS reading was $\approx 1.9 \times 10^{-5}$ mbar. In most deposition experiments the pressure of water vapor in the chamber was selected to be $\approx 8 \times 10^{-6}$ mbar.

A density of $\rho = 2.74 \times 10^{22}$ molecules cm^{-3},[24] has been used for the calculations of the amorphous film growth with eq 2. The estimated film thickness was always found to be in good agreement with the optical interference measurements as illustrated, for a typical series of measurements, in the lower panel of Figure 2. For the films deposited at 163 K a density $\rho = 3.11 \times 10^{22}$ molecules cm^{-3} was taken.[24] In this case evaporation can become more relevant and the different literature values[8,9,20,21,24,28,66] for ν_0 and E_d may introduce significant differences in the calculated growth rate. Using the data of Haynes et al.[21] ($\nu_0 = 2.8 \times 10^{30}$ molecules cm^{-2}, $E_d = 49.8$ kJ mol^{-1}), we obtain always a very good agreement with the corresponding optical interference measurements, as shown in the upper panel of Figure 2. Appreciably higher values of the evaporation rate in eq 2 would not account for the observations. With the parameters just mentioned, the accordance between the d values estimated from exposure and from optical interference, both for amorphous and crystalline films, do not differ by more than 10% over the whole range of thickness values (up to $\approx 5\ \mu$m) measured and lie within the mutual experimental uncertainty. For $P_g \approx 8 \times 10^{-6}$ mbar the growth rates were ≈ 1 nm s^{-1} for the amorphous films and ≈ 0.8 nm s^{-1} for the crystalline ones. For the deposition of the thickest films, rates close to 2 nm s^{-1} were employed.

4. Simulation Procedure

The reflectivity of a multilayer system at a given frequency can be calculated directly from the complex dielectric constant of each phase, using solutions to the Maxwell's equations to describe the intensity of the electromagnetic field on either side of each interface, and the absorption and phase change on traversing each phase. A general method for the calculation of reflection and transmission properties in a multiphase system can be found, for example, in ref 60. In particular, McIntyre and Aspens[59] have calculated the reflection−absorption spectra of a vacuum/absorbing dielectric film/metal system using Fresnel equations. For a three-phase system, the overall Fresnel coefficients for s- and p-polarization are given by

$$r^s_{123} = \frac{r^s_{12} + r^s_{23}\exp(-2i\beta)}{1 + r^s_{12}r^s_{23}\exp(-2i\beta)} \tag{3a}$$

and

$$r^p_{123} = \frac{r^p_{12} + r^p_{23}\exp(-2i\beta)}{1 + r^p_{12}r^p_{23}\exp(-2i\beta)} \tag{3b}$$

where r_{ij} are the Fresnel coefficients for the interface between phases i and j, and $\beta = 2\pi(d/\lambda)\sqrt{\hat{n}_2^2 - n_1^2\sin^2\theta_1}$ is the change in phase of the beam during one traversal of the absorber phase 2 of thickness d (see Figure 1).

The reflectance of a vacuum/ice/metal system as a function of the angle of incidence (θ_1) and film thickness (d) for s- and p-polarized radiation can be calculated as $R^s = |r^s_{123}|^2$ and $R^p = |r^p_{123}|^2$ respectively, and the total reflectance can be expressed as $R = R^s + R^p$. To compare with experimental results, the calculated spectra have been plotted in absorbance units (AU), where AU is defined as

$$\mathrm{AU}^s = -\log\left(\frac{R^s}{R^s_0}\right) \tag{4a}$$

$$\mathrm{AU}^s = -\log\left(\frac{R^p}{R^p_0}\right) \tag{4b}$$

$$\mathrm{AU} = -\log\left(\frac{R^s + R^p}{R^s_0 + R^p_0}\right) \tag{4c}$$

for s- polarized, p- polarized, and nonpolarized light, respectively. R_0 refers to the reflectance from the vacuum-metal interface (i.e., the bare substrate without ice). In the present work, we have applied these equations to vacuum/ice/aluminum and vacuum/ice/gold systems. *Mathematica* software was used to calculate de AU spectra for an incident angle of 75°.

For the simulation of RAIR spectra of ice films deposited at 163 K in the spectral region 6452−605 cm^{-1}, the empirical values of the real n and imaginary k parts of the complex refractive index of ice were taken from Toon et al.,[61] who derived them from transmission spectra of ice films deposited at 163 K. For the simulation of spectra of amorphous ice films in the spectral region 4000−620 cm^{-1}, the empirical values of n and k, for ice deposited at 77 K, reported by Leger et al.[35] were taken. The wavelength-dependent optical indices for metallic Al, Au, and Cu were taken from room-temperature values reported by Palik.[67] These metal optical data were fitted and the functions obtained were evaluated at the same wavenumbers as n and k of ice.

In the extreme cases of very thin or very thick ice films some approximations can be made to the reflection Fresnel coefficients defined in eqs 3a,b. For very thin films, when $d \ll \lambda$, a linear approximation of the exponential function in eq 3 can be applied. In our problem the substrate is a highly reflective metal and the ice film is weakly reflecting compared to the metal. In this case, the normalized reflectance change, $\Delta R/R_0$, can be written for s- and p-polarized light, respectively, as

$$\left(\frac{\Delta R}{R_0}\right)_s = 0 \tag{5}$$

and

$$\left(\frac{\Delta R}{R_0}\right)_p = -\frac{16\pi {n_1}^3 n_2 k_2 d \sin^2\theta_1}{({n_2}^2 + {k_2}^2)^2 \lambda \cos\theta_1} = -\frac{4{n_1}^3 n_2 \sin^2\theta_1}{({n_2}^2 + {k_2}^2)^2 \cos\theta_1}\alpha d \tag{6}$$

where $\Delta R = R - R_0$ is the increase in reflectance arising from the presence of the film and $\alpha = 4\pi k_2/\lambda$ is the absorption coefficient of the film. The normalized intensity change in transmission through the film is given by $-\alpha d$. The difference between this and the right-hand side of eq 6 is the enhancement factor. Shape differences between transmission and reflection−absorption spectra, for very thin films, are due to the frequency dependence of this enhancement factor. Equation 6 shows that the absolute value of the p-polarized normalized reflectance increases linearly with film thickness. In the frequency range of the OH stretching region of ice, around $\lambda = 3300\ cm^{-1} = 3\ \mu m$, this condition implies a film thickness $d \ll 3\ \mu m$. Zondlo et al.[40] found experimentally that the limit of the linear behavior of the absorbance RAIRS spectra of the OH stretch of crystalline ice with film thickness, is 50 nm. In the present work we have not studied in detail this very thin film region and, in the thickness range investigated, no linear behavior is observed.

In the opposite limit, when very thick films are deposited, $d \gg \lambda$, the phase factor β is very large, and the exponential function can be approximated to zero. In this case, eqs 3a,b are reduced to $r^s_{123} = r^s_{12}$ and $r^p_{123} = r^p_{12}$, respectively, where r^s_{12} and r^p_{12} are the Fresnel coefficients of a two-phase vacuum/ice system. The thickest films studied in present work are around $d = 5\ \mu m$. With this thickness, the exponential function, $\exp(-2i\beta)$, corresponding to 3400 cm^{-1} is effectively close to zero. It is expected that, in this frequency range, for a thickness of several microns, the reflectance will be dominated by the vacuum/ice, r_{12}, Fresnel coefficient.

5. Spectra and Simulations

Figure 3 shows the s-polarized, p-polarized, and nonpolarized spectra of an amorphous and a crystalline ice film deposited on an Au surface. The film thickness was determined to be 0.5 μm from interference measurements. Similar results (not shown) were obtained for ice films of the same thickness when deposited on an Al surface. The rest of the experiments described in this section were performed on both Au and Al substrates, and the results were always found to be very similar; therefore the spectra will not be duplicated in the presentation. All the spectral simulations presented in this section have been carried out using the Fresnel formulation described in the previous section, with the interference-measured film thickness, d, as input parameter.

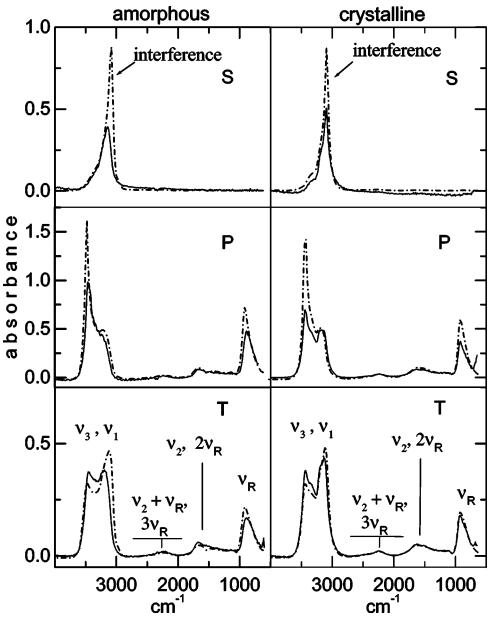

Figure 3. Experimental (solid lines) and simulated (dash lines) s- (S), p- (P), and nonpolarized (T) grazing-angle RAIRS spectra ($\theta_i = 75°$) for an amorphous (left column) and a crystalline (right column) water−ice film. Films were vapor-deposited on Au at 87 and 163 K, respectively. The film thickness, from optical interference measurements, was 0.5 μm. The location of an IR interference is marked with an arrow. Assignments of the main spectral features are presented: ν_1 and ν_3, symmetric and antisymmetric OH stretching, ν_2, bending, and ν_R hindered rotational lattice mode.

The main spectral features can be easily identified by comparison with the transmission spectra and assignments of the literature.[29,30] Strong absorptions between ≈2800 and 3600 cm^{-1} are essentially due to OH stretch vibrations (ν_1, ν_3). The weak feature at ≈2250 cm^{-1} has been assigned either to the combination band of the bending mode of water and the hindered rotational lattice mode ($\nu_2+\nu_R$) or to the third overtone of the hindered rotation ($3\nu_R$). The small peak at ≈1600 cm^{-1} is attributed to the bending mode of water (ν_2) possibly coupled with the second overtone of the hindered rotation ($2\nu_R$), and the large band at ≈900 cm^{-1} corresponds to the hindered rotational mode (ν_R). Except for the absorption in the OH stretch region the spectral features are absent in the s-polarized spectra, indicating that they correspond essentially to the excitation of molecular motions that generate transition dipole moments oriented perpendicular to the metal substrate, i.e., longitudinal optic (LO) modes of the solids. Spectra recorded using nonpolarized radiation are weaker than those recorded with p-polarization. This well-known effect is due to the nonadditive behavior of the absorbance,[68] reflected in eqs 4a,c. The spectra of the crystalline and amorphous solids show an overall similarity albeit with appreciable differences in the OH band shapes, which are more marked in the polarized spectra. As far as we know, a rigorous theoretical calculation relating the spectra with the respective ice structures and thus accounting for the observed band contours is not available yet. The simulations

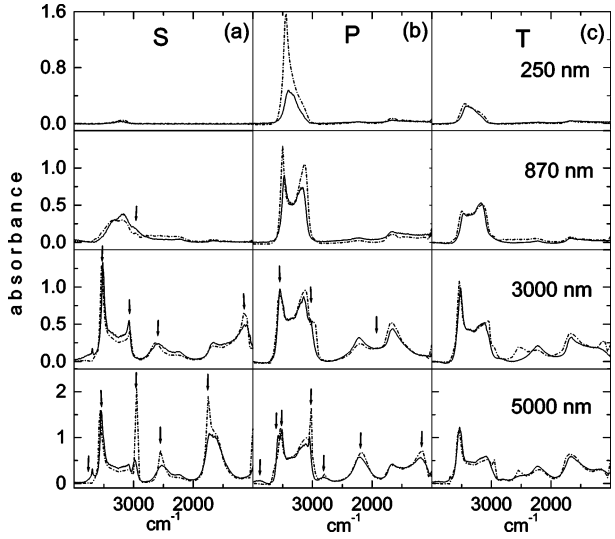

Figure 4. Comparison of experimental (solid lines) and simulated (dash lines) s-, p-, and nonpolarized grazing-angle RAIRS spectra ($\theta_i = 75°$) for amorphous water−ice films 0.25, 0.87, 3, and 5 μm thick. Ice films were vapor-deposited on Al at 87 K. Arrows show the locations of IR interferences (see Table 1).

with the Fresnel model and the empirical optical constants mentioned above reproduce globally well the measurements but give too large values at the most intense absorption peaks of the polarized spectra. In the s-polarized spectra the peak position coincides with that of an IR interference (see below).

A general overview of the evolution of the main features of the RAIR spectra with film thickness can be seen in Figure 4. In this Figure s-polarized, p-polarized, and nonpolarized experimental (solid lines) and calculated (dash lines) spectra of amorphous water-ice films are represented over the 1000−4000 cm^{-1} range.

The s-polarized spectra displayed in Figure 4a, show an almost negligible absorbance for the thinnest (250 nm) film, evidencing that in grazing-angle RAIRS this polarization component is effectively canceled by the so-called metal surface selection rule[57] (MSSR). When the film thickness increases, the MSSR is relaxed and absorption of s-polarized radiation, caused by the excitation of modes with transition dipole moment parallel to the ice surface (TO modes), is also observed. For films thinner than $\approx$1 μm this absorption, corresponding to the OH stretch, gives rise to a band with a maximum at $\approx$3150 cm^{-1}. For the geometric configuration of the present experiment (angle of incidence 75°), p-polarized radiation is enhanced near the metal surface and strong absorbance signals are observed even for thin films (see Figure 4b). For p-polarized light, and for film thickness lower than 1 μm, the highest peak in the OH stretch band is close to 3450 cm^{-1}, a frequency higher than that in s-polarized spectra. This frequency displacement between LO ant TO modes is in agreement with the interpretation of Whalley,[47] based on the LST relation, and with the more recent treatment of Buch and Devlin.[43] Initially, the intensity of the OH stretch band grows with increasing film thickness. When the film approaches 0.5 μm, the (polarized and nonpolarized) OH stretch bands get broader and develop shoulders that increase in intensity. For films thicker than 0.5 μm major changes are observed in all the OH stretch absorptions, especially in the polarized spectra. For $d > 1$ μm the RA spectra are affected by significant changes over the whole frequency range, with broad and intense peaks appearing and disappearing at different film thicknesses. These changes can be essentially explained by IR optical effects characteristic of the RAIRS

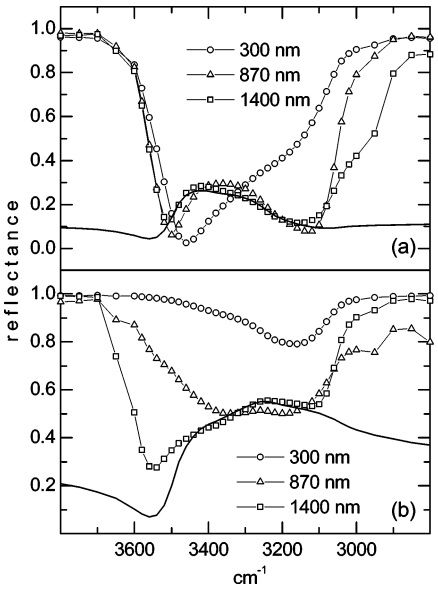

Figure 5. (a) Simulated p-polarized reflectance, as defined in section 4, for a vacuum/water−ice/Al system, $|r^p_{123}|^2$ (lines with symbols) and for a vacuum−ice system, $|r^p_{12}|^2$, (solid line). With increasing film thickness, some frequencies of the refracted light are completely absorbed by the ice film and the reflectance $|r^p_{123}|^2$ equals $|r^p_{12}|^2$. (b) Same as (a) but for s-polarized light.

technique and are not due to variations in the ice morphology. In general, the reflectivity, determined by the complex refractive index relating reflection and absorption, will show marked variations with thickness in the neighborhood of strong absorption bands.

The main optical effects determining the shape of the spectral features in the thicker films can be described in terms of saturation and interferences. In the p-polarized spectrum, the 3400 cm^{-1} peak of the OH band reaches a maximum intensity of $\approx$0.8−0.9 AU for $d \approx 500$ nm, and with increasing film thickness the rest of the band also saturates. At $d = 870$ nm a characteristic minimum can be seen on top of the OH stretch band. The intensity and shape of this minimum remains approximately constant for thicker films. As illustrated in Figure 5a, the frequency range of the minimum corresponds to a maximum of the IR p-polarized vacuum-ice reflection r^p_{12}, showing that the shape of the RA spectrum in this frequency interval is dominated by the IR reflection at the vacuum−ice surface and that the refracted component is absorbed completely by the ice. A similar effect is observed in the s-polarized spectra but in this case the OH stretch absorption first saturates at $\approx$3200 cm^{-1} (see Figure 5b).

A careful study of the evolution of a series of shifting peaks appearing at different frequencies for different film thickness, shows that they correspond to interferences. Destructive IR interferences lead to a decrease of the radiation arriving to the detector, and show up as peaks in the absorption spectra. The destructive interference wavelengths, λ, of s- and p-polarized light at grazing incidence and the corresponding ice film thickness can be approximately related through[63]

$$d = \frac{(m + 1/2)\lambda}{2\left[\frac{n_2}{\cos(\theta_2)} - n_1 \sin(\theta)\tan(\theta_2)\right]} \quad \text{with}$$

$$m = 0, 1, 2, \ldots \text{ (s-polarized light)} \quad (7)$$

and

$$d = \frac{(m\lambda)}{2\left[\frac{n_2}{\cos(\theta_2)} - n_1 \sin(\theta)\tan(\theta_2)\right]} \quad \text{with}$$

$$m = 0, 1, 2, \ldots \text{ (p-polarized light)} \quad (8)$$

where m represents the interference order. The main approximation used in the derivation of these equations is the assumption that the phase shift of the IR radiation in the ice−metal reflection is 180° for both s- and p-polarized light. This assumption is correct at all incidence angles for s-polarized radiation and it is also reasonable for p-polarized light at grazing-angle incidence.[69] Application of eqs 7 and 8 shows that the interferences corresponding to a given order, shift from high to low frequency with increasing film thickness. As an illustration of this behavior consider, for instance, the first-order interference, $S-1$, appearing at 2580 cm^{-1} in the s-polarized spectrum of a 3 μm amorphous film in Figure 4, and note that it is shifted to 1720 cm^{-1} when the film grows to 5 μm (see Table 1). All the interferences located in the experimental s- and p-polarized spectra of the present work have been assigned without ambiguity (see Figures 3, 4, 6, 8, and 9). The experimental and calculated positions of the IR interferences in Figures 4 and 6 are presented in Table 1. In the absence of polarization the spectral variations are not so drastic as those found for measurements with s- and p-polarized light. With increasing thickness the nonpolarized spectra show a gradual saturation in the OH stretch region with a marked peak at ≈3500 cm^{-1} caused, at least in part, by interferences. Over the rest of the spectral range studied the distortions due to the IR interferences are significantly smaller than in the polarized spectra and the characteristic absorptions of ice (see refs 29 and 30) and the corresponding assignments in these references and in Figure 3) are easily recognized. The small peak at ≈3700 cm^{-1}, commonly attributed to OH dangling bonds is also appreciable in the spectra of the thickest films even with the small scale of Figure 4. It is interesting to observe that this peak appears more neatly in the s-polarized spectra.

Polarized and nonpolarized RAIR spectra as a function of film thickness have been also recorded for crystalline ice layers deposited at 163 K. A selection of the RAIR spectra obtained for d up to 5.7 μm is presented in Figure 6, together with the corresponding Fresnel model simulations in broken lines. The general trends in the spectra of crystalline samples are analogous to those described for amorphous ice. For thin layers the suppression of s-polarized radiation due to the MSSR and the intensity enhancement for the p-polarized radiation are also observed. For $d > 500$ nm, the evolution of the RAIR spectra with film thickness is mostly dominated by the same optical effects (saturation and interferences) described above for the amorphous films. A close inspection of spectra of amorphous and crystalline films of comparable thickness shows indeed appreciable differences; some of them will be commented in the next section. At this point it is interesting to observe that the dangling bond feature at ≈3700 cm^{-1} clearly apparent in the spectra of the thickest amorphous films is not discernible in the spectra of the crystalline ones. The strong decrease of the dangling bond signal in the crystalline samples is related with the disappearance of the internal surfaces of the micropores upon crystallization.[40,44]

The spectra of Figures 4 and 6 were measured on an Al substrate. As indicated above, analogous measurements were performed on ice layers formed on a gold substrate under the same deposition conditions. The two sets of RAIR spectra bear a great similarity. Sometimes slight differences (<10%) in the absorbance, but not in the band shape are observed between the spectra of films of the same thickness recorded on the two metallic surfaces, but they are within the uncertainty of the thickness determination. The only difference worth noting corresponds to the IR interferences observed in the s-polarized spectra, which are more intense for ice grown on gold than for ice grown on aluminum. This peculiarity is also reproduced in the Fresnel calculations with the optical constants available in the literature for the two metals.[67] The effect is not very intense, and it is not appreciable in the p-polarized or nonpolarized spectra, where the IR interferences are weaker. The Au data are not shown for simplicity.

TABLE 1: Frequency Positions of IR Interferences in the Spectra of Figures 4 and 6[a]

90 K, amorphous ice				163 K, crystalline ice			
Pol-m	d (μm)	exp (cm^{-1})	cal (cm^{-1})	Pol-m	d (μm)	exp (cm^{-1})	cal (cm^{-1})
S-0	0.87	2800	2740	S-0	0.85	2800	2775
S-0	3	1100	1120	S-0	2.5	1200	1150
S-1	3	2580	2580	S-1	2.5	2870	2800
S-1	5	1720	1720	S-1	5.7	1400	1405
S-2	3	3070	3075	S-2	5.7	2290	2290
S-2	5	2530	2535	S-3	5.7	2790	2810
S-3	5	2975	2975	S-4	5.7	2990	3020
S-0	5	3515	3470	S-0	0.85	3300	3220
S-1	3	3550	3540	S-0	2.5	3490	3480
P-1	3	1880	1860	S-1	5.7	3510	3500
P-1	5	1170	1120	S-2	5.7	3615	3620
P-2	3	3035	2900	S-3	5.7	3950	4000
P-2	5	2150	2100	P-1	2.5	2150	2100
P-3	5	2810	2780	P-1	5.7	1100	1070
P-4	5	3050	3020	P-2	2.5	3030	3020
P-1	3	3530	3450	P-2	5.7	1860	1900
P-1	5	3515	3450	P-3	5.7	2570	2620
P-2	5	3570	3550	P-4	5.7	2940	2940
P-3	5	3950	3885	P-1	2.5	3580	3580
				P-1	5.7	3480	3470
				P-2	5.7	3545	3454
				P-3	5.7	3760	3760

[a] Pol: polarization of the IR radiation. *m:* interference order. *d:* thickness of the ice film. exp*:* experimental interference positions. cal*:* calculated interference positions (using eqs 7 and 8).

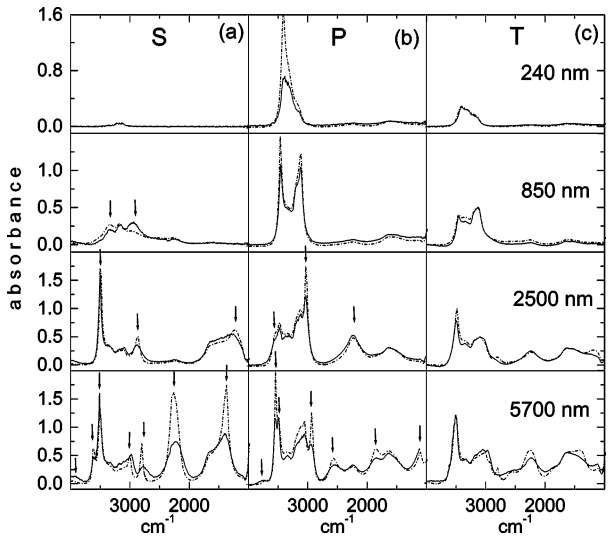

Figure 6. Comparison of experimental (solid lines) and simulated (dash lines) s-, p-, and nonpolarized grazing-angle RAIRS spectra ($\theta_i = 75°$) for crystalline water−ice films 0.24, 0.85, 2.5, and 5 μm thick. Ice films were vapor-deposited on Al at 163 K. Arrows indicate the position of the IR interferences (see Table 1).

The measured absorbance spectra are globally well reproduced by the Fresnel model of eqs 4a−c both for amorphous and crystalline ice (see Figures 3, 4, and 6). In general, the frequency and shape of the main IR absorptions as well as the effects of saturation and interferences, are well accounted for by this model, but some discrepancies are also worth noting. For relatively thin ($\leq$0.5 μm) films, both amorphous and crystalline, the calculated peak maximum in the OH stretch band of the polarized spectra is always more intense than the experimental one. In the polarized spectra of the thickest films, the locations and rough shapes of the measured interference features are well rendered by the model, but many of the corresponding maxima are largely overestimated. In all cases the best agreement between experiment and model calculations is obtained in the simulation of the nonpolarized spectra.

The reasons for the discrepancies just commented on are not entirely clear. As indicated in the Introduction, the lack of refinement of the simple model used for the simulation was pointed out by some authors.[37,40,63] The model was originally developed for homogeneous films and it is plausible that irregularities of the real samples could lead to distortions of the reflectance with respect to that of an ideal layer. The absence of flat parallel surfaces could indeed be the cause of the smaller intensity of the sharpest experimental peaks, which are associated with surface enhancement or with interferences. Overall, however, the differences between the present measurements and the model calculations are much smaller than those found in the literature.[37,40,63] Possible reasons for the larger discrepancies reported by other authors will be discussed in the next section. Some contribution to the differences between measurements and simulations could also come from the optical indices used. The optical constants of amorphous ice used to calculate the spectra were measured for ice deposited at 77 K,[35] a somewhat lower temperature than that of the present experiment (87 K). At each temperature slightly different water networks may be formed and that could lead to some changes in the band contours. In agreement with Toon et al.[61] we have assumed throughout this work that the 163 K vapor deposited ice is crystalline and have used their optical constants obtained from transmission IR spectra performed on ice deposited at the same temperature. Nevertheless, the morphology of polycrystalline ice samples may be determined, not only by the temperature, but also by the growing conditions. The deposition rate used by Toon et al. to grow the ice was 1.77 nm/s, faster than the $\approx$0.8 nm/s rate used in present work. Finally, experimental errors can also contribute to the observed discrepancies. In particular, the angle of incidence of the radiation (75°), which influences sensibly the absorbance intensity, is affected by an uncertainty of $\approx\pm$3°. Besides, the polarized spectra, where the larger discrepancies are found, are very sensitive to possible misalignments of the polarizer.

6. Comparison with Previous Works

In the following paragraphs and in Figures 7−10 representative RAIR spectra from the literature are compared to measurements of the present work and to Fresnel model simulations. Some of the previous articles include such simulations but given the disparity of results found in the publications, they have all been repeated here for consistency. All the simulations shown have been performed with eqs 4a−c using in each case the optical indices of amorphous[35] and crystalline[61] ice and of the corresponding metallic surfaces.[67]

Several groups have reported grazing angle RAIR spectra with d < 100 nm,[9,37,40,44] and some representative data from these

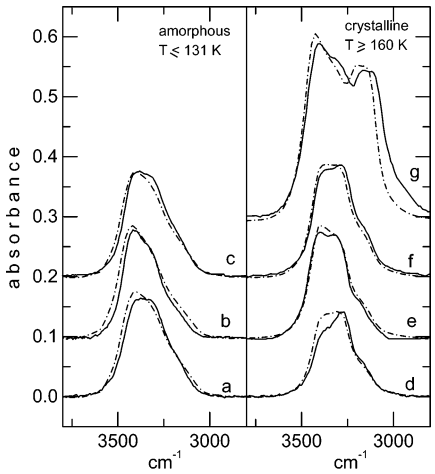

Figure 7. Comparison of experimental (solid lines) and simulated (dash lines) grazing-angle RAIRS spectra of amorphous and crystalline thin water−ice films (reported thickness <100 nm): (a) and (d) this work, 75° incidence angle, Au substrate, 87 and 163 K, Fresnel simulation for d = 80 nm; (b) and (e) Mitlin and Leung,[44] 83° incidence angle, 131 and 160 K, Cu substrate, and Fresnel simulation for d = 50 nm; (c) and (f) Jenniskens et al.,[9] 75° incidence angle, 80 and 160 K (35 s annealing), Au substrate, Fresnel simulation for d= 80 nm; (g) same as (f) for 3300 s annealing and simulation with d = 350 nm.

references are displayed in Figure 7 together with spectra of the present work. All these spectra were recorded with nonpolarized IR radiation. The spectra of the left panel correspond to amorphous films with substrate temperatures lower than 131 K, and those of the right panel to polycrystalline layers with substrate temperatures higher than 160 K. Important changes in the OH stretch band region are clearly appreciable. Note that a larger variability is observed in the spectra of the polycrystalline samples. For such thin films, the accurate determination of d is difficult. The optical interference method described in the Experimental Section cannot be used reliably and estimates based on exposure become less precise. Therefore, the simulations have been performed using d as an adjustable parameter.

The spectrum (a) of Figure 7 was measured in this work on a thin film deposited at 87 K with an incidence angle of 75°. The best Fresnel model simulation of this spectrum was obtained with d = 80 nm in good agreement with the estimate based on the deposition rate (77 nm). The spectrum (b) of this figure was recorded by Mitlin and Leung[44] on a film deposited at 131 K with an incidence angle of 83°. In this case, the simulation led to a thickness of 50 nm. This value is also in reasonable agreement with the estimation from the deposition rate (0.43 nm s^{-1}) and deposition time (120 s) of this experiment. It is worth noting that Mitlin and Leung report this deposition rate for a water pressure of 1×10^{-6} Torr in the chamber, which would be at variance with the predictions of eq 2, but as noted by the authors, this pressure corresponds to an uncalibrated gauge whereas the deposition rate was determined from optical interference measurements. In these two spectra the calculated absorptions are somewhat wider and extend toward higher frequencies than the measured ones but overall the band shapes and intensities are reproduced satisfactorily. As can be seen, the spectrum of ref 44 is somewhat narrower but has a slightly higher and sharper maximum than that of the present work despite the smaller thickness. The Fresnel model calculations indicate that these features can be justified by the difference in the angle of incidence of the IR radiation in the two experiments. Spectrum c of Figure 7 was taken from ref 9 and corresponds to a thin ice film deposited at 80 K. This experiment was performed with an angle of incidence of 75° and consequently

the band shape is very similar to that of spectrum a. The Fresnel model simulation of spectrum c yields a thickness of 80 nm as compared with the 20 nm estimated in ref 9.

Spectrum d of Figure 7 was measured in our laboratory and corresponds to an ice film deposited on a substrate held at 163 K and thus assumed to be polycrystalline. The simulation yields a thickness of 50 nm in very good agreement with the value obtained from calculated deposition and evaporation rates by means of eq 2. Spectrum e was reported by Mitlin and Leung for a polycrystalline film deposited at 160 K and also having a thickness of 50 nm, as estimated both from modeling and from exposure. In comparison with the amorphous film spectra previously commented on, those of polycrystalline layers (d and e) show a relative increase in absorption intensity around 3270 cm^{-1} The same trend is also obtained in the model calculations. Again in this case the different incidence angle could explain at least in part the different band shapes of the spectra (d) and (e),

Spectra f and g are from ref 9 and were obtained by annealing at 160 K the amorphous thin film corresponding to spectrum c of this figure. Spectrum f is obtained after 35 s annealing and spectrum g after 3300 s. From parallel measurements of transmission electron microscopy, the authors of ref 9 conclude that after annealing, the initially amorphous ice is transformed into a film containing cubic polycrystalline ice, and also noncrystalline domains formed either by an amorphous solid or a viscous liquid. During the transformation process, the new film is assumed to become optically flatter with a lower diffuse reflectance and a higher specular reflectance that could explain the drastic changes observed in the band shape upon prolonged annealing. However, Mitlin and Leung did not observe this behavior but found instead that the spectra of the samples deposited at 131 K followed by annealing to 165 K were essentially identical to the spectra of the samples prepared by direct deposition at 160 K. It should be noted that spectrum g presents not only a pronounced change in the band shape but also a marked increase in the absorbance. In fact, this spectrum is best simulated with a thickness of 350 nm. A possible explanation for this result could be an actual slow growth ($\approx$0.1 nm s^{-1}) of the film caused by a slight excess in the confinement pressure used to prevent film sublimation, which is already appreciable at 160 K. In fact, a gradual increase in the absorbance is observed in the series of spectra recorded by Jenniksens et al.[9] during the process of annealing (see Figure 2 of ref 9). Spectrum f recorded just after 35 s of annealing is in good agreement with spectrum d recorded in this work with the same angle of incidence and corresponding to a film directly deposited at 163 K.

RAIR spectra of ice films with d values between 0.1 and $\approx$1 μm can be found in refs 9, 37, 40, 44, and 63. A comparison between nonpolarized spectra of amorphous and crystalline films from this work and from the experiments of Mitlin and Leung is presented in Figure 8 for films of $\approx$100 and $\approx$1200 nm. Spectral simulations performed with eq 4c are also included in the figure. The strong effect of the incidence angle on the intensity and shape of the RAIRS spectra is apparent and also the good accord between measurements and model calculations. For the 100 nm films, the agreement is good for both amorphous and crystalline samples, whereas for the 1200 nm layers some differences are found in the maxima of the OH stretch band. Note how the absorption maximum at about 2300 cm^{-1} is enhanced by the presence of an interference, which is more marked for the 83° angle of incidence. For intermediate values of the thickness (see Figures 3, 4, and 6 and ref 44) the

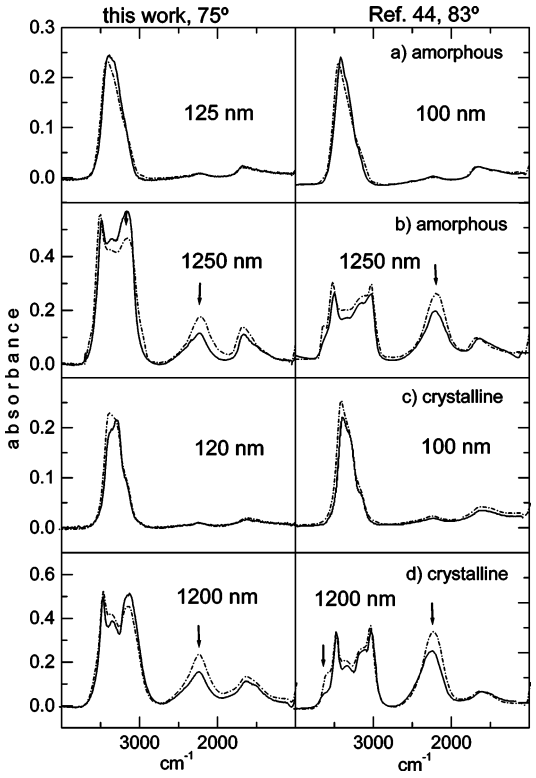

Figure 8. Comparison of experimental (solid lines) and simulated (dash lines) nonpolarized grazing-angle RAIRS spectra of amorphous and crystalline water−ice films. The left panel correspond to experimental results of this work and the right panel to the results of Mitlin and Leung.[44] Arrows indicate the positions of IR interferences.

agreement between the measurements and the simulations is of the same order. Mitlin and Leung report in their work the existence of a thickness range (100−250 nm) in which the OH stretch band of the spectra of polycrystalline films is saturated and does not change in either shape or intensity. Calculations performed with the Fresnel model for the angle of incidence of their experiment account for this behavior. For the angle of incidence of the present experiment saturation of the absorbance is neither found experimentally nor predicted by the model over the thickness interval studied.

Spectra of crystalline ice layers with $d = 0.1$, 0.5, and 1 μm of Zondlo et al.[40] recorded with s- and p-polarized light are represented in Figure 9 and compared with present work measurements for the same d values. In both cases the thickness values reported were derived from optical interference measurements and the deposition rate was the same. A general similitude in the band shapes of corresponding spectra from the two experiments is observed in all cases and the various band contours are reasonably well simulated by the Fresnel model. The main differences between the two sets of measurements are found in the absorption intensity and can be traced back mostly to the different angle of incidence. As already observed, the model does not always reproduce accurately the intensity absorption features distorted by interferences and tends to overestimate the values of the absorbance in the presence of sharp peaks. Note the significant influence of interferences in the shape of the s-polarized spectra. The present simulation is in better accord with the experimental results of Zondlo et al.[40] than that presented by the authors in their original paper, which gave the same band shapes but absorbance values smaller by a factor of 2. The reason for this difference is not clear taking into account that the same model has been used in both cases. In ref 40 the authors give (E_1^+/E_1^-) instead of $|E_1^+/E_1^-|^2$

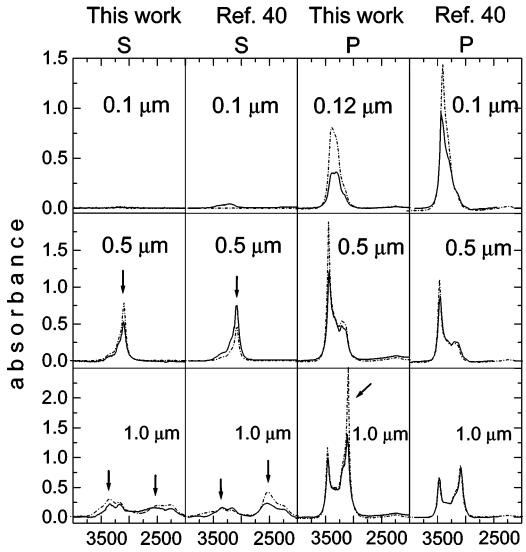

Figure 9. Comparison of present s- and p- polarized RAIR spectra of crystalline ice on Al with previous results by Zondlo et al.[40] Solid lines correspond to experimental measurements and the dashed lines to Fresnel simulations. s-polarized spectra are represented in the two left columns and p-polarized spectra in the two right ones. Note that the angle of incidence in this work is 75° whereas that of Zondlo et al. is 83°. Arrows indicate the position of interferences.

(following their notation) as the expression for the reflectance; if this expression has actually been used in the calculations this would account for the mentioned factor of two difference. Equationss 4a,b have also been applied to the simulation of the s- and p-polarized spectra reported by Robinson et al.[63] (not represented for brevity), and the level of agreement was found to be similar to that shown in Figure 9.

Grazing angle nonpolarized RAIR spectra of ice films with purported thickness values of several microns can be found in refs 9 and 37. The OH stretch region of the spectra of ref 9 is represented in Figure 10 together with similar measurements performed in our laboratory. In both experiments the incidence angle was 75°, the deposition temperature close to 80 K and the deposition surface gold. For each spectrum the corresponding Fresnel model simulation is also shown. In spite of some discrepancies the spectra can be simulated reasonably well by the model calculations. Note that the calculated absorption in the lower frequency peak (≈3150 nm) is appreciably larger than the experimental one for film thickness 0.5-0.6 μm. This enhancement of the simulated signal coincides with the presence of an interference. The measurements of this work (left panel) have been simulated using the *d* values determined from optical interference, whereas for those of Jenniskens et al.[9] (right panel) *d* was used as a fitting parameter. In ref 9 no estimates of the film thickness of the individual spectra were provided, but they were assumed to lie between 0.05 and 10 μm by comparison with data from IR transmission. However, given the essential differences between the processes of transmission and reflection−absorption, such a comparison is not warranted in principle. On the other hand, the IR transmission spectra for ice films with a thickness of several microns[61] lead to much higher absorbances than those reported in ref 9. The present measurements and the simulations of the Fresnel model indicate, however, that the highest *d* value corresponding to the spectra of refs 9 and 37 should hardly surpass 0.5 μm. Spectra of films up to 5 μm thick were presented and discussed previously in this work (see Figures 4 and 6). In the article of Horn et al.[37] Fresnel model calculations for s- and p-polarized RAIR spectra using the optical indices of Toon et al.[61] were also presented.

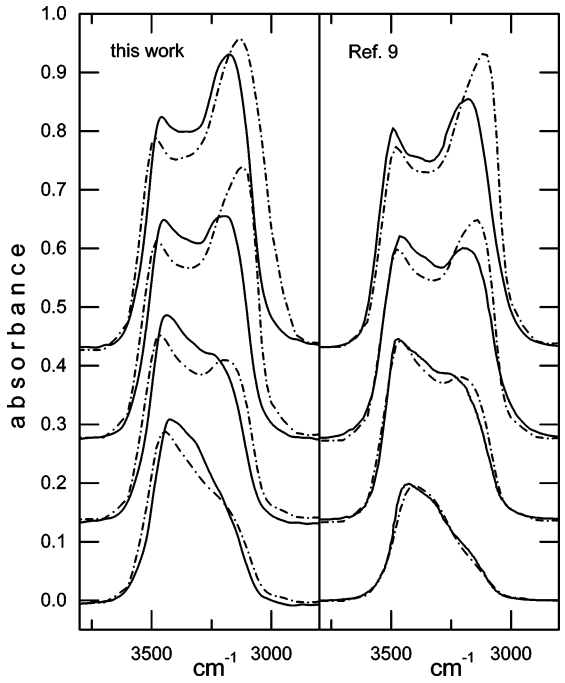

Figure 10. Comparison of experimental (solid lines) and simulated (dash lines) nonpolarized 75° RAIRS spectra of amorphous water−ice films vapor deposited on Au at 87 K (left panel) and 80 K (right panel). Simulations of the experimental spectra of this work (left panel) used thickness values of 0.25, 0.375, 0.5, and 0.675 μm, determined from optical interference. In the simulations of the experimental spectra of ref 9 (right panel) *d* was used as fitting parameter, and best fit values of 0.1, 0.35, 0.5, and 0.55 μm were found.

Zondlo et al.[40] noted a discrepancy between the (known) film thickness corresponding to their measurements (see above) and the much larger thickness values associated by Horn et al. to the same band shapes. The calculations of Horn et al. were performed for an angle of incidence of 75° and are thus directly comparable to this work, where very similar band shapes and absorbances are obtained with a thickness 10 times smaller. This fact and the good agreement between the present simulations and experimental measurements carried out on films of known thickness suggests that the calculations of Horn et al. are essentially the same as those of this work but were probably wrongly labeled in their Figure 5. The simulations of nonpolarized RAIRS data (eq 4c) cannot be directly compared with their results because Horn et al. presented only the sum of their s- and p-polarized spectra.

7. Summary and Conclusions

Extensive measurements of grazing-angle RAIR spectra of amorphous and crystalline ice layers deposited from the vapor phase on gold and aluminum surfaces have been performed using polarized and nonpolarized IR radiation. The present measurements extend the previously available data toward higher film thickness values (up to 5 μm) and provide a systematic set of polarized spectra over the thickness range studied.

The influence of the surface on the RAIR spectra can be used advantageously to suppress or enhance the signals from different vibrational modes of the solid, providing valuable data for a rigorous theoretical investigation. Increasing the film thickness certainly diminishes the influence of the substrate, but the RAIR spectra of ice films never look like transmission spectra due mostly to absorption saturation and to IR interferences that lead to substantial signal distortions. In any case, a correct modeling of the optical effects inherent to the technique is indispensable

for a sound interpretation of the spectra. The results are found to be very similar on the two types of surfaces (Au and Al) investigated. Contrary to some assets in the literature, it is found that the application of a simple Fresnel model developed for homogeneous dielectric layers on a metallic surface,[59] together with empirical optical indices from the literature,[35,61] gives a good global account not only of the band shapes but also of the intensity of the RAIR spectra over the whole film thickness range studied in this work, at least in the experiments performed with nonpolarized radiation. For this type of measurements the present results corroborate the conclusion of Mitlin and Leung[44] who indicated that Fresnel model simulations could be used as a semiempirical estimates of the film thickness. In the spectra recorded with polarized radiation the accord is worse and the model often overestimates the magnitude of the absorbance of sharp intense peaks. A reanalysis of previous literature data with this model shows a similar degree of agreement and can help to clarify existing discrepancies.

Acknowledgment. This work was financed by the MCyT of Spain under Grant REN 2000-1557 CLI. We are indebted to P. Gutierrez for help in the early stage of the work and to J. M. Castillo and J. Rodriguez for constant support and technical advice.

References and Notes

(1) Wayne, R. P. *Chemistry of Atmospheres*, 3rd ed.; Oxford University Press: Oxford, U.K., 2000.
(2) Finlayson-Pitts, B. J.; Pitts, J. N., Jr. *Chemistry of the Upper and Lower Atmosphere*; Academic Press: San Diego, 2000.
(3) Solomon, S. *Rev. Geophys*. **1999**, *37*, 275.
(4) van Dishoek, E. F.; Blake, G. A. *Annu. Rev. Astron. Astrophys*. **1998**, *36*, 317.
(5) Ehrenfreund, P.; Charnley, S. B. *Annu. Rev. Astron. Astrophys*. **2000**, *38*, 427.
(6) Fletcher, N. H. *The Chemical Physics of Ice*; Cambridge University Press: Cambridge, U.K., 1970.
(7) Jenniskens, P.; Blake, D. F. *Science* **1994**, *265*, 753.
(8) Speedy, R. J.; Debenedetti, P. G.; Smith, R. S.; Huang, C.; Kay, B. D. *Chem. Phys*. **1996**, *105*, 240.
(9) Jenniskens, P.; Banham, S. F.; Blake, D. F.; McCoustra, M. R. S. *J. Chem. Phys*. **1997**, *107*, 1232.
(10) Narten, A. H.; Venkatesh, C. G.; Rice, S. A. *J. Chem. Phys*. **1976**, *64*, 1106.
(11) Langel, W.; Fleger, H. W.; Knözinger, E. *Ber. Bunsen-Ges. Phys. Chem.* **1994**, *98*, 81.
(12) Kohl, I.; Mayer, E.; Hallbrucker, A. *Phys. Chem. Chem. Phys*. **2000**, *2*, 1579.
(13) Materer, N.; Starke, U.; Barbieri, A.; van Owe, M. A.; Somorjai, G. A.; Kroes, G.-J.; Minot, C. *Surf. Sci*. **1997**, *381*, 190.
(14) Wenzel, J.; Linderstrom-Lang, C. Rice, S. A. *Science* **1975**, *187*, 428.
(15) Kolesnikov, A. I.; Li, J.; Parker, S. F.; Eccleston, R. S.; Loong, C.-K. *Phys. Rev. B* **1999**, *59*, 3569.
(16) Li, J.-C. *J. Chem. Phys*. **1996**, *105*, 6733.
(17) Hinch, B. J.; Dubois, J. *Chem. Phys*. **1992**, *96*, 3262.
(18) Braun, J.; Glebov, A.; Graham, A. P.; Menzel, A.; Toennies, J. P. *Phys. Rev. Lett*. **1998**, *80*, 2638.
(19) Hallbrucker, A.; Mayer, E.; Johari, G. P. *J. Phys. Chem.* **1989**, *93*, 4986.
(20) Sandford, S. A.; Allamandola, L. J. *Icarus* **1988**, *76*, 201.
(21) Haynes, D. R.; Tro, N. J.; George, S. M. *J. Phys. Chem.* **1992**, *96*, 8502.
(22) Wornsop, D. R.; Fox, L. E.; Zahniser, M. S.; Wolfsy, S. C. *Science* **1993**, *259*, 71.
(23) Schaff, J. E.; Roberts, J. T. *J. Phys. Chem.* **1996**, *100*, 14151.
(24) Brown, D. E.; George, S. M.; Huang, C.; Wong, E. K. L.; Rider, K. B.; Smith, R. S.; Kay, B. D. *J. Phys. Chem.* **1996**, *100*, 4988.
(25) Brown, D. E.; George, S. M. *J. Phys. Chem.* **1996**, *100*, 15460.
(26) Chaix, L.; van den Bergh, H.; Rossi, M. J. *J. Phys. Chem.* **1998**, *102*, 10300.
(27) Livingston, F. E.; George, S. M. *J. Phys. Chem. A* **1998**, *102*, 10280.
(28) Koehler, Brigit G. *Int. J. Chem. Kinet*. **2001**, *33*, 295.
(29) Bertie, J. E.; Labbe, H. J.; Walley, E. *J. Chem. Phys*. **1969**, *50*, 4501.
(30) Hardin, A. H.; Harvey, K. B. *Spectrochim. Acta* **1973**, *29A*, 1139.
(31) Venkatesh, C. G.; Rice, S. A.; Bates, J. B. *J. Chem. Phys*. **1975**, *63*, 1065.
(32) Sivakumar, T. C.; Rice, S. A.; Sceats, M. G. *J. Chem. Phys*. **1978**, *69*, 3468.
(33) Bergren, M. S.; Schuh, D.; Sceats, M. G.; Rice, S. A. *J. Chem. Phys*. **1978**, *69*, 3477.
(34) Hagen, W.; Tielens, A. G. G. M.; Greenberg, J. M. *Chem. Phys*. **1981**, *56*, 367.
(35) Leger, A.; Gauthier, S.; Deforneau, D.; Rouan, D. *Astron. Astrophys*. **1983**, *117*, 164.
(36) Callen, B. W.; Grifiths, K.; Norton, P. R. *Surf. Sci. Lett*. **1992**, *261*, L44.
(37) Horn, A. B.; Banham, S. F.; McCoustra, M. R. S. *J. Chem. Soc., Faraday Trans*. **1995**, *91*, 4005.
(38) Givan, A.; Loewenschuss, A. Nielsen, C. *J. Vibr. Spectrosc*. **1996**, *12*, 1.
(39) Delzeit, L.; Devlin, J. P.; Buch, V. *J. Chem. Phys*. **1997**, *107*, 3726.
(40) Zondlo, M. A.; Onasch, T. B.; Warshavsky, M. S.; Tolbert, M. A.; Mallick, G.; Arentz, P.; Robinson, M. S. *J. Phys. Chem. B* **1997**, *101*, 10807.
(41) Kanno, M. A.; Tomikawa, K.; Mishima, O. *Chem. Phys. Lett*. **1988**, *293*, 412.
(42) Schriver-Mazzuoli, L.; Schriver, A.; Hallou, A. *J. Mol. Struct*. **2000**, *554*, 289.
(43) Buch, V.; Devlin, J. P. *J. Chem. Phys.* **1999**, *110*, 3437.
(44) Mitlin, S.; Leung, K. T. *J. Phys. Chem. B* **2002**, *106*, 6234.
(45) Bode, G. *Ann. Phys*. **1909**, *30*, 326.
(46) Rao, I. K. *Proc. R. Soc. A* **1931**, *130*, 489.
(47) Whalley, E. *Can. J. Chem.* **1977**, *55*, 1977.
(48) Ritzhaupt, G.; Smyrl, N.; Devlin, G. P. *J. Chem. Phys*. **1976**, *64*, 435.
(49) Rowland, B.; Devlin, J. P. *J. Chem. Phys*. **1991**, *94*, 812.
(50) Rowland, B.; Fisher, M.; Devlin, J. P. *J. Chem. Phys*. **1991**, *95*, 1378.
(51) Horn, A. B.; Chesters, M. A.; McCoustra, M. R. S.; Sodeau, J. R. *J. Chem. Soc. Faraday Trans*. **1992**, *88*, 1077.
(52) Schaff, J. E.; Roberts, J. T. *J. Phys. Chem.* **1994**, *98*, 6900.
(53) Lyddane, R. H.; Sachs, R. G.; Teller, E. *Phys. Rev.* **1941**, *59*, 673.
(54) McGraw, R.; Madden, W. G.; Bergren, M. S.; Rice, S. A. *J. Chem. Phys*. **1977**, *69*, 3483.
(55) Madden, W. G.; Bergren, M. S.; McGraw, R.; Rice, S. A. *J. Chem. Phys*. **1978**, *69*, 3497.
(56) Rice, Stuart A.; Bergren, Michel, S.; Belch, Alan C.; Nielson, Glenn. *J. Phys. Chem.* **1983**, *87*, 4295.
(57) Suëtaka, W. *Surface Infrared and Raman Spectroscopy: Methods and Applications*; Plenum: New York and London 1995.
(58) Greenler, R. G. *J. Chem. Phys*. **1966**, *44*, 310.
(59) McIntryre, J. D. E.; Aspens, D. E. *Surf. Sci*. **1971**, *24*, 417.
(60) Born, M., Wolf, E., Eds. *Principles of Optics*; Pergamon Press Ltd: Oxford, U.K., 1959.
(61) Toon, O. B.; Tolbert, M. A.; Koehler, B. G.; Middelebrook, A. M. *J. Geophys. Res*. **1994**, *99* (D12), 25, 631.
(62) Yen, Y.-S.; Wong, *J. Phys. Chem.* **1989**, *93*, 7208.
(63) Robinson, M. S.; Mallick, G.; Spillman, J. L.; Carreon, P. A.; Shalloo, S. *Appl. Opt.* **1999**, *38* (1), 91.
(64) Carrasco, E.; Castillo, J. M.; Escribano, R.; Herrero, V. J.; Moreno, M. A.; Rodríguez, J. *Rev. Sci. Instrum*. **2002**, *73*, 3469.
(65) Berland, R. S.; Haynes, D. R.; Foster, K. L.; Tolbert, M. A.; George, S. M.; Toon, O. B. *J. Phys. Chem.* **1994**, *98*, 4358.
(66) Sack, N. J.; Baragiola, R. A. *Phys. Rev. B* **1993**, *48*, 9973.
(67) Palik, E. D., Ed. *Handbook of the Optical Constants of Solids*; Academic: Toronto, 1985.
(68) Song, Y. P.; Petty, M. C.; Yarwood, J. *Vibr. Spectrosc.* **1991**, *1*, 305.
(69) Hoffmann, F. *Surf. Sci. Rep.* **1983**, *3*, 107.